

Mineralogical Studies and Radioactivity of the Top Meter Depth of the Egyptian Black Sand, El-Dibeh, Port Said Governorate, Northern Coast of Egypt

A. M. El-Shafey*

Nuclear Material Authority, P.O. Box 530 Maadi, Cairo, Egypt.

Received: 21 Feb. 2022, Revised: 22 Mar. 2022, Accepted: 24 Mar. 2022.

Published online: 1 May 2022.

Abstract: The study area lies on the Mediterranean Sea coast, about 8 Km east of El-Manzala Lake between longitudes $32^{\circ} 3' 41.39'' - 32^{\circ} 7' 51.46''$ E and latitudes $31^{\circ} 21' 52.92'' - 31^{\circ} 19' 49.27''$ N. Mineralogical Investigation was conducted in El-Dibeh, Port Said Governorate beach area to detect economic minerals. Fifty-one samples collected on a grid pattern of 400m parallel to shoreline and 50 m perpendicular to shoreline was made to evaluate an area of 8 km length and 150 m width. Using a definite mineralogical analysis procedure program, the various heavy mineral contents in the different collected samples were calculated. Using both of wet gravity concentration, low and high intensity magnetic separation and the high-tension electrostatic separation techniques, each of the individual six economic minerals, leucosene and cassiterite can be obtained in a high-grade concentrate with accepted grade and recovery. The resource tonnage for each concerned economic mineral in the different sectional area is calculated for the drilled top meter depth zone to be: (92.640 ilmenite, 58.720 Magnetite, 3.840 garnet, 17.760 Leucosene, 12.000 zircon, 4.640 rutile, 0.736 monazite and 20.960 Green silicates) a total reserve of thousand tons. The average concentrations of (eU, ppm) and (eTh, ppm) reach up to 1.41 and 4.66 ppm, respectively. In addition, the potassium concentration (K, %), attains an average of 0.60%. Also, the calculated values of absorbed dose were found to be ranged between 6.47 and 32.22 (nGy/h) with an average value 21.54 (nGy/h). This is lower than the world average value of 60 nGy/h. The average value of the total effective dose from all terrestrial gamma radiations is 0.174(mSv/y).

Keywords: Mineralogical Studies, Northern Coast.

1 Introduction

The Egyptian black sand placer deposits are distributed along the Mediterranean Sea coast and the red sea. The Egyptian black sand extends between Abu Qir to the west and Rafah to the [1], [2] and [3]. It well represented in 4 localities namely, the beach area of Rosetta, north Sinai coastal area, the beach area of Damietta and the coastal sand dunes of El-Burullus-Baltim area. Fig. (1).

Actually, the black sand deposits consider one of the most important minerals resources in Egypt and contain strategic and economic heavy minerals, which are needed either for nuclear industry or other metallurgical and engineering industries. The Egyptian black sands along the Mediterranean Sea coast are known for their enhanced natural radiation environment, due to radiogenic heavy minerals such as monazite, radioactive zircon, thorite and uranothorite. The main part of the Egyptian beach minerals

comes from basement rocks of the upper reaches of the Nile River and its main tributaries as, Blue Nile (60%), Atbara River (26%) Ethiopian highland and White Nile (14%) Equatorial plateau, [19].

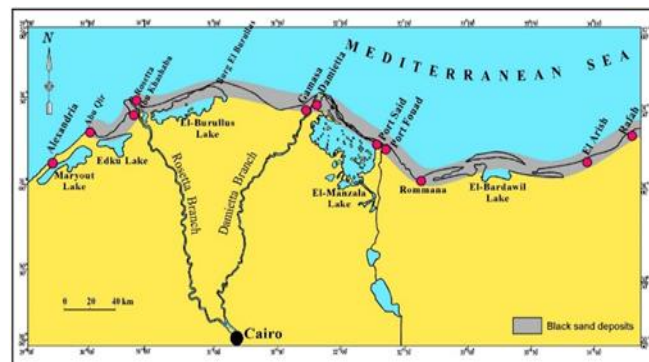


Fig.1: Distribution of the black sand deposits in the northern coast of Egypt.

*Corresponding author e-mail: abdelshafey48@gmail.com

2 Study Areas

The study area lies on the Mediterranean Sea coast, about 8 Km east of El-Manzala Lake between longitudes $32^{\circ} 3' 41.39'' - 32^{\circ} 7' 51.46''$ E and latitudes $31^{\circ} 21' 52.92'' - 31^{\circ} 19' 49.27''$ N. The coastal plain of this area is nearly rectangular in shape, covers about 8 km stretch parallel to shoreline with 150 m width nearly perpendicular to the shoreline (Fig. 2).

It is flat and less than 1 meter height above sea level. The area is free of stacks and coves and no clear cusps are observed. Sea water covers the beach during winter stormy conditions and high tide periods. The present paper deals with the evaluation of economic minerals of El Dibeh beach area vertically and horizontally, as well as the calculating the mineral resource of the studied beach area.



Fig. 2: Satellite map showing location of field samples.

3 Experimental

3.1 Sampling and Methodology

The study area is 8 Km long parallel to the shoreline and 150 m width nearly perpendicular to the shoreline. Fifty-one samples were obtained from the studied coastal plain area to a depth of one meter at the intersection of a grid pattern $400\text{m} \times 50\text{m}$ nearly parallel and perpendicular to the shoreline. Then, the area of study was covered by 51 samples taken along three profiles (A, B and C) (Fig. 2). Each profile is parallel to each other and to shoreline and comprises (21, 18 and 12) boreholes, respectively; and the first profile (A) is far from shoreline by about 10 meters. Each representative sample was weighted and poured inside a calibrated cylinder and compacted well by shaking to be analogous to the field deposit. The weight of the sand was divided by its volume to obtain the apparent specific gravity [20]. Each field sample was split into two halves using John's Splitter. One of them was kept as a reference sample and the second was subjected to splitting again to obtain a representative sample weighing about 50 grams for the different analyses while the rest was used as composite sample. Each composite sample was quartered by rotary splitter to a proper weight (about 50 gm). The quartered sample was weighed, and then washed with water, followed

by decantation to get rid of slimes and salts. About 5ml of ammonium hydroxide was added for the disaggregation of the clay particles. Samples with organic matter were treated with few drops of hydrogen peroxide 30%. The treated samples were sieved and washed several times using 50μ screen to determine the amount of slime. Both the oversize and the undersize fractions were dried and weighted. The slime free fraction was separated using bromoform (Sp. gr. 2.89) into heavy and light fractions. Methylene Iodide (specific gravity of 3.3 gm/cm^3) was used to reduce the size of the obtained heavy fraction by the separation of the light-colored silicates in the float sub-fraction while the dark colored silicates as well as the heavy economic minerals were sunk. The weight percentages of each heavy fraction, in the corresponding original raw sample while the dark colored silicates as well as the heavy economic minerals were sunk. The weight percentages of each heavy fraction, in the corresponding original raw sample while the dark colored silicates as well as the heavy economic minerals were sunk. The weight percentages of each heavy fraction, in the corresponding original raw sample were calculated.

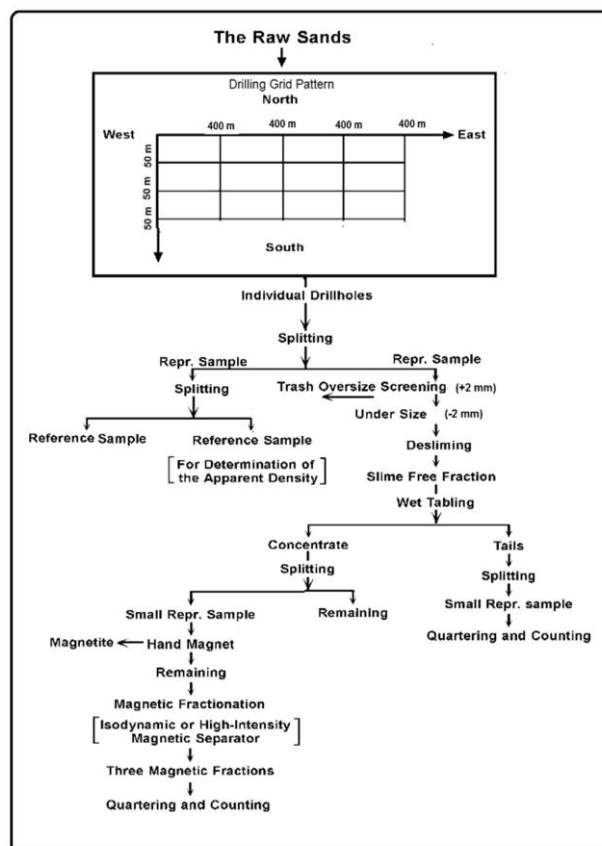


Fig.3: A flowsheet showing the drilling grid pattern for collecting raw sand samples and the various treatments of the mineralogical analysis.

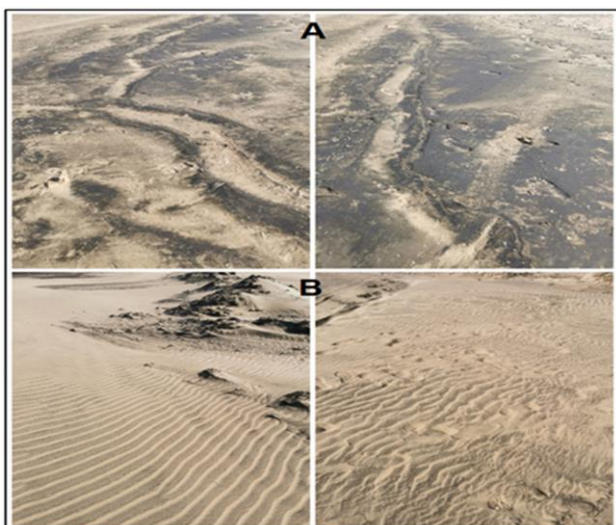


Fig. 4: A-Photograph showing the highly concentrated black. B-Photograph showing diluted homogenous sands of the studied area.

A hand magnet was used to separate magnetite from the heavy Methylene Iodide fraction. The individual magnetite free samples were treated by laboratory Frantz Isodynamic Magnetic Separator Model (L-1) with longitudinal slope of 20o, side slope 5o and at ampere values of 0.2, 0.5, 1.0 and 1.5. Then, five fractions were obtained. Each fraction was weighted and about 1000 grains were counted under the binocular microscope. The weight percent of each mineral in every fraction was calculated using the equation of [21]. A flowsheet showing the drilling grid pattern for collecting raw sand samples and the various treatments of the mineralogical analysis shown in Fig. 3. Photograph showing the highly concentrated black sand and diluted homogenous sands of the studied area showing in Fig. 4. The contents of each mineral in any original composite sample were determined by adding its contents in the different counted subtractions Binocular and optical microscope, Environmental Scanning Electron Microscope (ESEM) performed detailed mineralogical investigation and identification. A Philips (XL30) ESEM, equipped with an energy dispersive X-ray spectrometer (EDX), was used for scanning electron micrographs of the surface features of economic minerals. In addition, semi-quantitative (EDX) were performed for determination of the chemical composition of the economic minerals. All analyses were carried out in the laboratories of the Nuclear Materials Authority, Egypt.

4 Results

4.1 Apparent Specific Gravity

It was noticed that the apparent density values vary from 1.43 to 1.81 gm/cm³ with an average value of 1.60 gm/cm³ for the top meter depth raw sand samples. The apparent

density values along samples in the studied area are shown in Table (1), figure (5).

4.2 Determination of Slime Content

It was noticed that the slime contents for samples vary from 0.81 to 3.09 wt. %, with an average value of 1.36 wt. %. The contents of slimes values along samples in the studied area are shown in Table (1) & figure (5).

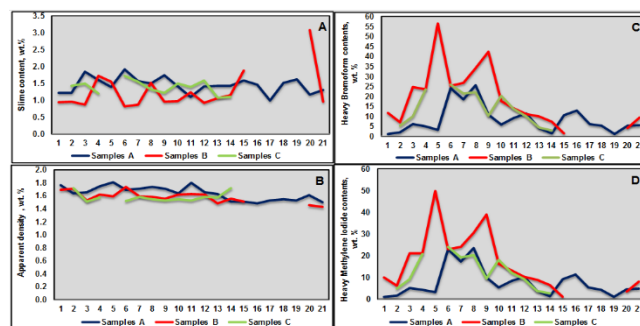


Fig.5: Line Charts showing A- The slime contents of samples along the studied area, B-; the measured average apparent density for samples, C- The heavy bromoform contents for samples and D-The heavy methylene iodide contents of samples along the studied area; wt. % = weight percent.

4.3 Heavy Liquids Separation

A representative sample weighing about 50 gm from each collected drilled sample was taken and subjected to a process of heavy liquid separation using bromoform solution (sp. gr.=2.81 gm/cm³). The bromoform was added to the sample. The quantity of the added liquid was enough to make the solid/liquid ratio suitable to give a complete freedom for all the particles to settle or float. The sample was thoroughly stirred in the liquid using a glass rod and left at rest. After the suitable time at rest, each sample was separated into a float layer and a sink layer with a clear liquid layer in-between. The heavy fraction of bromoform was taken on a filter paper in a precipitating funnel and the float or the light fraction was taken on another filter paper in another precipitating funnel. The two fractions were left to complete the filtration. The remaining bromoform in the bores and the thin film coating the particles of both the heavy and light fractions was washed with acetone several times till the two fractions becomes clean from any bromoform traces. Both light and heavy fractions were dried, weighed and the obtained heavy fractions during the bromoform separation were subjected to Methylene Iodide (3.3 gm/cm³). The separation was carried out to reduce the size of the heavy fraction by the separation of the light-colored silicates in the float layer, while the darker colored heavy economic minerals were sinking. Each bromoform heavy fraction was put in a separating funnel and a suitable amount from Methylene Iodide was added to permit each particle to freely sink or float. Both heavy and light

fractions were washed with acetone, dried, weighted and their percentages were calculated relative to the original sample weight. The results are shown for profiles (A, B and C) in Tables (1, 2 and 3), and Fig 5 (C and D) showing the heavy bromoform contents for samples and D-The heavy methylene iodide contents of samples along the studied area.

Table 1: The measured average of the slime and apparent density contents for samples in the studied area.

The measured average of the slime for Samples in the studied area.			The measured average of apparent density for samples in the studied area				
Samples	Profile A	Profile B	Profile C	Samples	Profile A	Profile B	Profile C
1	1.22	0.94		1	1.76	1.69	
2	1.22	0.96	1.42	2	1.64	1.71	1.72
3	1.85	0.87	1.5	3	1.66	1.53	1.51
4	1.6	1.73	1.2	4	1.75	1.62	1.57
5	1.4	1.55		5	1.81	1.59	
6	1.92	0.81	1.73	6	1.69	1.74	1.52
7	1.56	0.86	1.55	7	1.71	1.59	1.58
8	1.5	1.52	1.32	8	1.74	1.58	1.55
9	1.74	0.96	1.22	9	1.71	1.56	1.53
10	1.41	0.98	1.5	10	1.64	1.62	1.55
11	1.1	1.23	1.4	11	1.8	1.63	1.53
12	1.41	0.92	1.58	12	1.66	1.62	1.58
13	1.43	1.06	1.08	13	1.63	1.48	1.57
14	1.42	1.14	1.09	14	1.51	1.56	1.72
15	1.59	1.89		15	1.51	1.51	
16	1.47			16	1.48		
17	0.99	1.13		17	1.53	1.52	
18	1.52			18	1.55		
19	1.62			19	1.53		
20	1.16	3.09		20	1.61	1.46	
21	1.31	0.95		21	1.5	1.43	
Average	1.45	1.26	1.38	Average	1.64	1.58	1.58

The obtained individual heavy Methylene Iodide fractions were subjected to a process of magnetite separation using a standard hand magnet. The treated sample is spread on a large sheet of clean paper. A small hand magnet was dripped in the spread sample and passes across it, the separated magnetite was then transferred to another clean paper. The step was repeated several times until the treated sample becomes completely free of magnetite. The separated magnetite was weighed and its percentage relative to the weight of the original sample was calculated and quoted in Table (2 to 4). Contents of the individual economic minerals, leucoxene and green silicates of the drilled top meter depth samples of the first profile (A) of the studied area in wt. %.

4.4 Electromagnetic Fractionation

The magnetite free heavy parts were subjected to magnetic fractionation using the Frantz Isodynamic Separator modal, (L-1). The selected separation electric currents are 0.2, 0.5, 1.0 and 1.5 ampere. These magnetic field strengths were chosen to separate the opaque particles into three sub-parts; ilmenite particles in the highly magnetic sub-part, altered ilmenite in the next magnetic sub-part and the rest opaque

Table 2: The results of heavy liquid separation and

Samples A	Samples Wt. g	Heavy Br. Wt. %	Heavy M.I Wt. %	Magnetite Wt. %	Ilmenite Wt. %	Garnet Wt. %	Leucoxene Wt. %	Zircon Wt. %	Rutile Wt. %	Monazite Wt. %	Green Silicates wt. %
A1	57.79	1.25	1.96	0.23	0.58	0.03	0.13	0.08	0.03	0.004	0.19
A2	59.75	1.93	1.67	0.48	0.87	0.02	0.15	0.10	0.04	0.008	0.26
A3	59.90	6.16	5.29	1.35	2.77	0.12	0.55	0.37	0.09	0.022	0.86
A4	44.90	5.02	4.42	1.10	2.36	0.05	0.53	0.25	0.10	0.018	0.60
A5	45.26	3.36	3.16	1.01	1.55	0.05	0.30	0.17	0.07	0.015	0.20
A6	57.52	24.11	22.91	6.03	12.06	0.24	2.17	1.69	0.60	0.084	1.21
A7	11.75	18.43	17.32	4.98	9.03	0.37	1.29	1.11	0.46	0.065	1.11
A8	51.06	25.54	23.50	6.77	12.01	0.51	2.30	1.28	0.51	0.089	2.04
A9	15.79	11.02	10.03	2.81	4.96	0.22	0.99	0.66	0.33	0.039	0.99
A10	63.72	6.00	5.46	1.38	2.88	0.09	0.60	0.36	0.12	0.024	0.54
A11	58.98	9.04	8.32	2.49	3.89	0.18	0.81	0.63	0.27	0.032	0.72
A12	55.53	11.57	10.41	3.24	4.74	0.23	1.27	0.64	0.23	0.035	1.16
A13	60.39	4.16	3.74	0.92	2.00	0.08	0.37	0.25	0.10	0.017	0.42
A14	54.33	1.40	1.27	0.32	0.65	0.03	0.13	0.10	0.04	0.005	0.13
A15	55.93	10.46	9.31	2.09	5.44	0.05	0.94	0.52	0.21	0.042	1.15
A16	59.08	12.97	11.48	4.02	5.19	0.26	1.04	0.65	0.26	0.045	1.49
A17	59.09	6.05	5.51	1.63	2.72	0.09	0.58	0.30	0.15	0.021	0.54
A18	60.98	5.16	4.44	0.85	2.48	0.10	0.57	0.31	0.10	0.018	0.72
A19	64.49	1.21	1.11	0.30	0.59	0.03	0.10	0.06	0.02	0.004	0.10
A20	66.08	5.29	4.60	1.11	2.43	0.11	0.53	0.29	0.11	0.021	0.69
A21	17.95	5.61	4.77	1.01	2.52	0.11	0.62	0.34	0.14	0.020	0.84
Average		8.37	7.61	2.10	3.89	0.14	0.76	0.48	0.19	0.030	0.76

Table 3: The results of heavy liquid separation and Contents of the individual economic minerals, leucoxene and green silicates of the drilled top meter depth samples of the Second profile (B) of the studied area in wt. %

Samples B	Samples Wt. g	Heavy Br. Wt. %	Heavy M.I Wt. %	Magnetite Wt. %	Ilmenite Wt. %	Garnet Wt. %	Leucoxene Wt. %	Zircon Wt. %	Rutile Wt. %	Monazite Wt. %	Green Silicates wt. %
B1	44.65	11.65	10.02	1.57	6.06	0.23	1.05	0.82	0.23	0.041	1.63
B2	53.39	6.95	6.36	1.95	2.99	0.14	0.70	0.42	0.14	0.021	0.59
B3	55.73	24.61	21.04	5.17	11.32	0.62	1.85	1.48	0.49	0.111	3.57
B4	54.93	23.66	21.06	7.10	9.70	0.47	1.89	1.18	0.59	0.071	2.60
B5	54.86	56.68	49.88	15.30	24.66	1.13	3.97	3.40	1.13	0.198	6.80
B6	59.71	25.22	22.95	7.06	11.10	0.63	2.27	1.26	0.50	0.076	2.27
B7	66.18	26.84	24.16	8.05	11.54	0.54	2.01	1.34	0.54	0.094	2.68
B8	54.64	34.29	30.51	10.97	13.20	0.89	2.74	2.06	0.69	0.086	3.77
B9	19.35	42.59	38.97	13.20	18.31	0.43	3.83	2.13	0.85	0.192	3.62
B10	59.28	17.53	16.13	5.08	7.71	0.35	1.40	1.05	0.44	0.053	1.40
B11	57.47	14.26	13.19	4.42	5.99	0.36	1.00	0.93	0.43	0.050	1.07
B12	60.87	11.21	10.20	3.36	4.60	0.22	1.12	0.62	0.22	0.034	1.01
B13	61.20	9.95	9.05	2.88	4.28	0.20	0.80	0.60	0.25	0.025	0.90
B14	19.09	7.30	6.50	1.79	3.50	0.15	0.51	0.44	0.15	0.022	0.80
B15	12.39	1.33	1.13	0.23	0.67	0.03	0.11	0.07	0.03	0.003	0.20
B16	-----	-----	-----	-----	-----	-----	-----	-----	-----	-----	-----
B17	19.92	1.05	0.94	0.27	0.45	0.03	0.09	0.06	0.03	0.004	0.10
B18	-----	-----	-----	-----	-----	-----	-----	-----	-----	-----	-----
B19	-----	-----	-----	-----	-----	-----	-----	-----	-----	-----	-----
B20	18.55	4.02	3.46	0.60	1.99	0.06	0.40	0.28	0.10	0.014	0.56
B21	16.94	9.28	8.07	2.13	3.99	0.19	0.83	0.60	0.28	0.032	1.21
Average		18.25	16.31	5.06	7.89	0.36	1.48	1.04	0.39	0.063	1.93

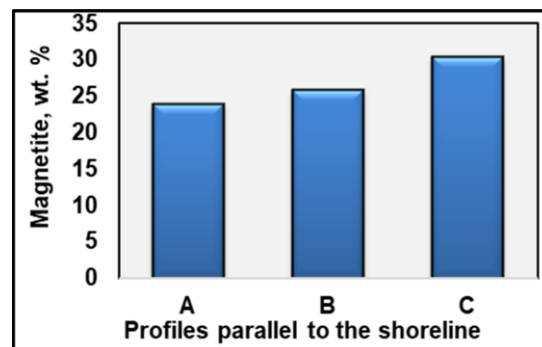


Fig.6: Graphic representation showing the average percentages of magnetite along three profiles parallel to the shoreline.

particles represent opaque rutile [22]. Also, the magnetic fractionation used to separate monazite from zircon particles into two different magnetic sub-parts. The obtained sub-fractions after magnetic fractionation were weighed and their frequencies were calculated relative to the weight of the original sample and represented in Figure 6.

4.5 Microscopic Investigation

Each free magnetite sub-fraction was subjected to microscopic examination to identify and count the different heavy economic minerals. The microscopic investigation of the studied samples was carried out under the binocular stereomicroscope and transmitted polarizing light microscope. A representative sufficient amount of minerals particles was taken by quartering from each magnetic sub-fraction and sprinkled on a glass slide, to be ready for the microscopic investigation. About 1000 mineral particles were identified and counted, from different microscopic fields covering the entire prepared slide. The frequency of each present mineral in the slide was calculated by multiplying the number of its particles by both its specific gravity and by one hundred. The product was divided by the sum of the products of the number of each present mineral particle by its specific gravity. The weight of each mineral in the different magnetic sub-fraction was calculated and summed to represent the total mineral weight in the sample. The frequency of each mineral in the original sample was calculated and the results were tabulated in Tables (2 to 4).

5 Results and Discussion

5.1 Distribution of Economic Minerals

The heavy Methylene Iodide fraction contains the six economic minerals; magnetite, ilmenite, zircon, rutile, garnet and monazite in addition to leucoxene, light and green silicate minerals. In these concentrated black sands. The distribution of economic minerals is correlated by their specific gravities, their grain sizes or even their grain shapes and also the location of their occurrences. Investigating the contents of the different individual economic minerals and green silicates in tables (2 to 4), ensures that the content for each of these minerals increase in profiles B, C and A respectively through the area of study are shown in Fig. 6. The calculated different economic minerals and green silicates of the various drilled samples in the studied area are shown in Tables (2 to 4). It was detected that the correlation between the heavy mineral's contents and each of the other individual economic minerals are shown in Fig. (7). The correlation coefficients are 0.99, 0.99, 0.93, 0.98, 0.99, 0.98, 0.97 and 0.95 for magnetite, ilmenite, garnet, leucoxene, zircon, rutile, monazite and green silicates. The average content for

each economic mineral and Green Silicates along the studied area. The average content for each economic mineral and Green Silicates along the studied area showing in Fig. 8.

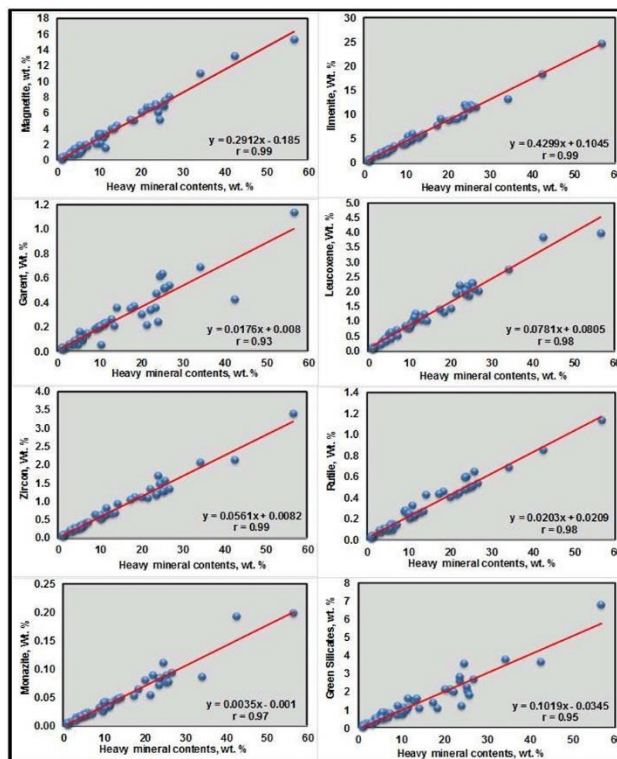


Fig.7: Scatter plot diagram showing the heavy mineral contents and each of the individual economic minerals for the drilled samples of the area of study: magnetite, ilmenite, garnet, Leucoxene, zircon, rutile, Monazite and green silicates; wt. % = weight percent.

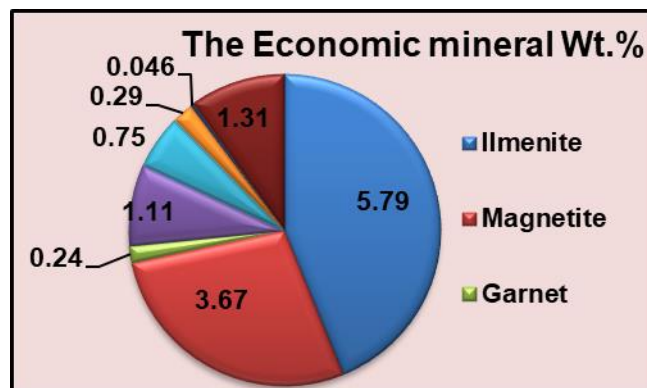


Fig. 8: The average content for each economic mineral and Green Silicates along the studied area.

Due to the relatively lower specific gravity and coarser grain sizes, garnet content may be variable according to the extent of erosion. Hence, garnet has the lowest correlation coefficient value with heavy Methylene Iodide fraction content. It is obvious that there are direct relations between

the heavy mineral's contents and each of the individual economic minerals and green silicates. In general, as the economic (heavy) mineral component content increases in the heavy mineral contents, as its correlation coefficient increases.

5.2 Estimation of the Economic Mineral Reserves

The calculated average weight percentages of the economic minerals, and green silicates for the studied area are estimated by computing the following values:

- The average apparent density of the sand samples;
- Volume of the studied area by multiplying length x width x depth,
- The tonnage of the stream sediments by multiplying the volume of the studied area by the average apparent density of the raw sand Tables 5.
- The reserves of the economic minerals by multiplying the tonnage for the raw sand of the studied area by the calculated weight % of each mineral. The total reserve of the economic minerals and green silicates in the studied area reaches up to 211296 tons of the area of study; Tables 6. The mineral resource tonnage for each concerned economic mineral in the different sectional area is calculated as shown in Table 6. From the table, this contains: 92640 ilmenites; 58720, magnetite; 3840, garnet; 17760, Leucoxene; 12000, zircon; 4640, total rutile, 736; monazite and 20960, green silicates, in tons. The economic minerals reserve is shown in the Tables 6.

Table 5: Volume, apparent density and tonnage of the raw sand of studied area.

Volume (m ³) (Length x width x depth)	Apparent Density Of raw sands (ton/m ³)	Tonnage Of raw sand (tons)
(A) 8000 x50x1= 400,000	1.60	1,600,000
(B) 7,200x50x1= 360,000		
(C) 4,800x50x1= 240,000		

Table 6: The average content and resource tonnage for each economic mineral and Green Silicates along the studied area.

The Economic mineral	The average content wt. %	Resource (tons)
Ilmenite	5.79	92640
Magnetite	3.67	58720
Garnet	0.24	3840

Leucoxene	1.11	17760
Zircon	0.75	12000
Total Rutile	0.29	4640
Monazite	0.046	736
Green Silicates	1.31	20960
Economic Minerals Content	13.22	211296

5.3 Radiometric Investigations

According to the used sampling grid pattern 400m×50m nearly parallel and perpendicular to the shoreline., 51 measured sites were obtained along 3 profiles (A, B & C), The measured elements include K (%), eU in (ppm) and eTh in (ppm) are shown in Table 7. Fig.9. Using the GS 512 gamma ray spectrometer the readings of the gamma ray spectrometry were measured to illustrate the horizontal distribution of the gamma ray spectrometry in the study area.

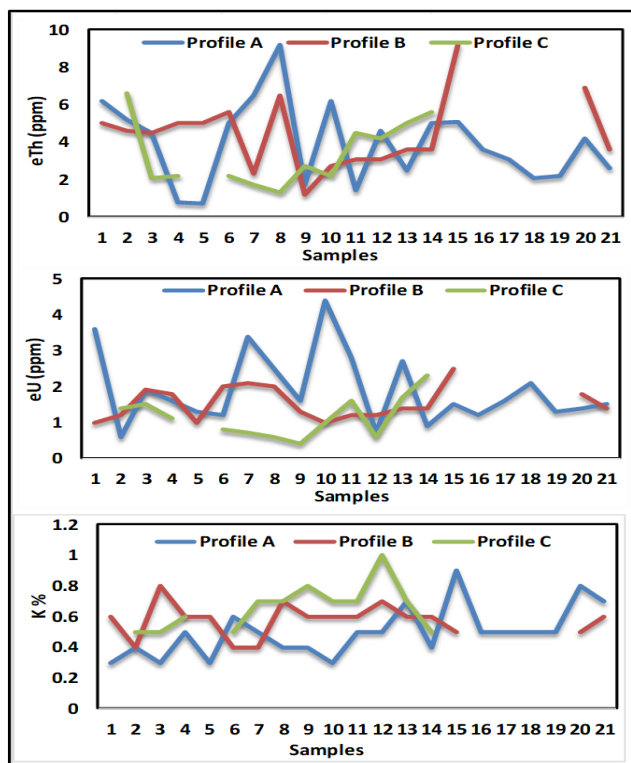


Fig.9: Graphic representation of the measured eTh (ppm), eU (ppm) and K (%) along 3 profiles (A, B & C).

From Table 7, it was observed that the uranium concentration (eU ppm) varies from 0.7 to 11.2 ppm, while the calculated average of the uranium concentrations is 1.40

ppm. The thorium concentration (eTh ppm) varies from 0.2 to 10.4 ppm and the calculated average of the thorium concentration is 4.66 ppm for the studied area. Potassium (K) concentration in weight percent (K %), varies from 0.2 to 0.9 % with average value of 0.60%. From the graphic representation of the measured eTh (ppm), eU (ppm) and K (%) along the three profiles (A, B and C), it was observed that, there are is no any relation between eTh, eU readings, which indicate their presence in discrete minerals. Potassium has moderate positive correlation with uranium suggesting its adsorption on clay minerals Th has ill-defined relation with potassium, indicating that its presence in refractory minerals. Inter element relations between radionuclides: A- eTh-eU, B- eU-K, and C- eTh-K shown in Fig.10

Table 7: The measured K (%), U (ppm) and Th (ppm) contents along profile A, B and D of the studied area using the GS 512 gamma ray spectrometer.

Samples No	Profile A			Profile B			Profile C				
	K (%)	eU (ppm)	eTh (ppm)	Samples No	K (%)	eU (ppm)	eTh (ppm)	Samples No	K (%)	eU (ppm)	eTh (ppm)
1	0.3	3.6	6.2	1	0.6	1.0	5.0	1	-	-	-
2	0.4	1.8	6.9	2	0.4	0.1	4.6	2	0.2	11.2	0.2
3	0.3	1.9	4.5	3	0.8	1.9	4.5	3	0.5	11.0	0.5
4	0.5	1.6	0.2	4	0.6	1.8	5.0	4	0.7	6.6	0.7
5	0.3	1.3	0.7	5	0.6	1.0	5.0	5	-	-	-
6	0.6	1.2	5	6	0.4	2.0	5.6	6	0.8	1.4	2.4
7	0.5	3.4	8.9	7	0.4	2.1	2.3	7	0.8	1.6	5.5
8	0.4	2.5	9.2	8	0.7	0.0	6.5	8	0.6	1.1	10.4
9	0.4	1.6	1.7	9	0.6	1.3	1.2	9	0.9	0.5	9.6
10	0.3	4.4	6.2	10	0.6	1.0	2.7	10	0.8	4.7	6.6
11	0.5	2.8	0.2	11	0.6	1.2	3.1	11	0.7	2.2	7.8
12	0.5	0.7	4.6	12	0.7	1.2	3.1	12	0.9	2.6	6.6
13	0.7	2.7	2.5	13	0.6	1.4	3.6	13	0.8	2.4	6.8
14	0.4	2	5	14	0.6	1.4	3.6	14	0.8	1.6	5.5
15	0.9	0.8	5.1	15	0.5	2.5	9.2	15	-	-	-
16	0.5	1.2	3.6	16	-	-	-	16	-	-	-
17	0.5	1.6	3.1	17	0.8	1.4	3.8	17	-	-	-
18	0.5	2.1	2.1	18	-	-	-	18	-	-	-
19	0.5	1.3	2.2	19	-	-	-	19	-	-	-
20	0.8	1.4	4.2	20	0.5	4.8	10.2	20	-	-	-
21	0.7	1.5	2.6	21	0.6	1.4	3.6	21	-	-	-
Min.	0.3	0.1	0.2	Min.	0.4	0.0	1.2	Min.	0.2	0.5	0.2
Max.	0.9	4.4	11.9	Max.	0.8	4.8	10.2	Max.	0.9	11.2	10.4
Av.	0.5	1.76	4.18	Av.	0.59	1.53	4.59	Av.	0.71	0.93	5.22

5.3.1 Absorbed Dose

The total absorbed dose rate of the study area along 21 profiles perpendicular to the shoreline.as well as minimum, maximum and average values of total absorbed dose rate of each profile were calculated and shown in Table 8. In general, the total absorbed dose rate of the study area varies between 6.47 (nGyh-1) and 32.22 (nGyh-1) with average value of 21.54(nGyh-1).

5.3.2 Outdoor Effective Dose

The annual effective doses are determined as follows according to [23]. {Eex, out (mSv/y) =Ab.Dose (nGyh-1) x 8760 (h/y) x 0.2 x 0.7 x 10-6} Time in hours for a year, [8760 (h/y)]. the outdoor effective dose rate of the study area varies between 0.008 (mSv/y) and 0.04(mSv/y) with average value of 0.26(mSv/y) shown in Table 8.

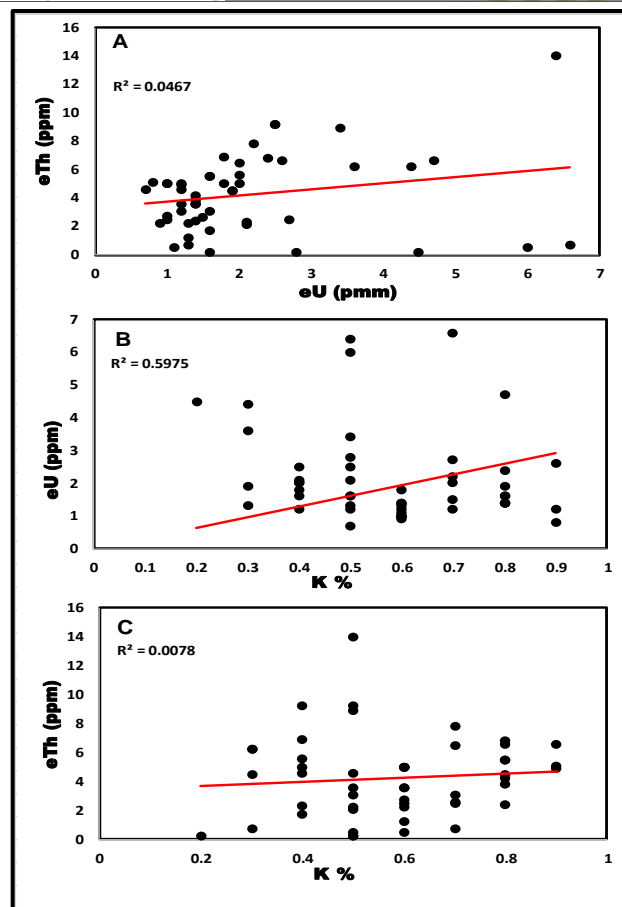


Fig.10: Inter element relations between radionuclides: A- eTh-eU, B- eU-K, and C- eTh-K.

5.3.3 Indoor Effective Dose

Eex, indoor (mSv/y) =Ab.Dose (nGyh-1) x 1.4 x 8760 (h/y) x 0.8 x 0.7 x 10-6} the indoor effective dose rate of the study area varies between 0.044 (mSv/y) and 0.22 (mSv/y) with average value of 0.148 (mSv/y) as shown in Table 8.

The total annual effective external dose Eex, total (mSv/y) is the sum of Eex, out (mSv/y) and Eex, indoor (mSv/y). The total annual effective external dose rate of the study area varies between 0.052 (mSv/y) and 0.261(mSv/y) with average value of 0.174(mSv/y) shown in Table 8. The average values of outdoor, indoor and total effective doses in (mSv/y) in study area along various square kilometers are shown in Table 8 and graphically represented in Fig.11. The average values of Eex, out, Eex, ind and Eex, total in the study area are 0.026, 0.148 and 0.174 (mSv/y) respectively. The average effective dose from the radiation emitted from the beach sands (and the construction materials that come from it) is approximately 0.174 mSv a year.

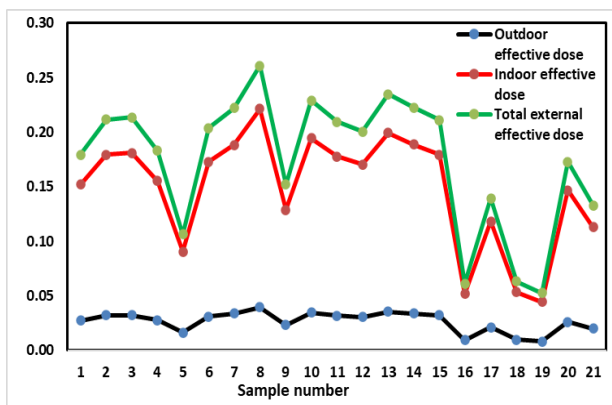


Fig. 11: Graphic representation of the measured showing the average values of outdoor, indoor and total effective doses in (mSv/y) in study area.

It is obvious that our findings are in general agreement with the worldwide measured value. The worldwide effective dose for the whole population from external terrestrial radiation is (0.5) mSv/year, [23].

Table 8: The total absorbed dose rate, average values of outdoor, indoor and total effective doses in (mSv/y) along 21 samples nearly perpendicular to the shoreline.

Samples. No.	Absorbed dose	Outdoor effective dose	Indoor effective dose	Total external effective dose
1	22.16	0.027	0.152	0.179
2	26.13	0.032	0.179	0.211
3	26.38	0.032	0.181	0.213
4	22.61	0.028	0.155	0.183
5	13.14	0.016	0.090	0.106
6	25.17	0.031	0.173	0.204
7	27.42	0.034	0.188	0.222
8	32.22	0.040	0.221	0.261
9	18.76	0.023	0.129	0.152
10	28.32	0.035	0.194	0.229
11	25.89	0.032	0.178	0.210
12	24.78	0.030	0.170	0.201
13	29.01	0.036	0.199	0.235
14	27.50	0.034	0.189	0.223
15	26.09	0.032	0.179	0.211
16	7.56	0.009	0.052	0.061
17	17.21	0.021	0.118	0.139
18	7.79	0.010	0.054	0.063
19	6.47	0.008	0.044	0.052
20	21.35	0.026	0.147	0.173
21	16.41	0.020	0.113	0.133
Min.	6.47	0.008	0.044	0.052

Max.	32.22	0.040	0.221	0.261
Ave	21.54	0.026	0.148	0.174

6 Economic Heavy Minerals:

6.1 Magnetite (Fe_2O_3 , Fe_3O_4).

Magnetite represents 27 wt. % of the total economic minerals. Its content varies between 0.23 – 15.30 wt. % with average value of 3.67 wt. %. The Egyptian beach magnetite grains has dull black colour of brownish and reddish appearance the EDX/BSE images of Magnetite of study area ESEM were shown in figure 12. They are always impure magnetite grains, exhibiting different types of internal texture of intergrowths and solid solutions with ilmenite and ulvospinel. A considerable number of grains are characterized by martitization and maghematization. They have generally irregular shape where subangular and subrounded grains are present beside octahedron crystals. The Egyptian beach magnetite shows evidence of oxidation with its low Fe^{++}/Fe^{+++} ratio, lower magnetic susceptibility and low specific gravity (= 4.760). A significant feature is the rather high titanium content; 12-13 % TiO_2 according to [24] and up to 18% TiO_2 according to [10] and [11]. Highly ferromagnetic grains nearly have abnormal spherical shape and are composed mainly of iron oxide.

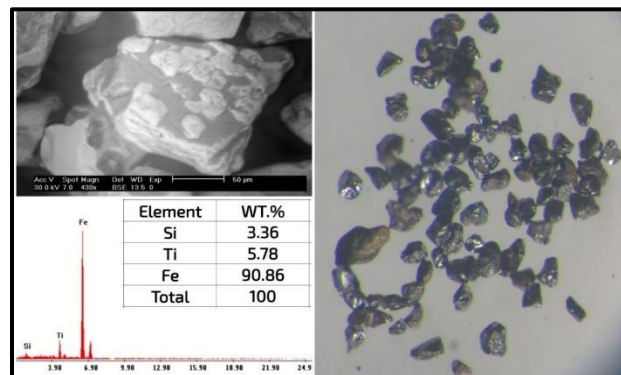


Fig.12: EDX semi-quantitative analyses and BSE images of octahedral magnetite crystal.

6.2 Ilmenite ($FeTiO_3$)

Ilmenite represents the main constituent in the heavy economic minerals, it represents more than 43 wt. % of the total economic minerals. Its content varies between 0.45 – 24.66 wt. % with average value of 5.79 wt. %. It is mostly black with bluish or violet tint. Some altered grains are dull black. Most of ilmenite grains are irregular in shape, angular to subangular and some grains are rounded. The examination under reflected light microscope showed that ilmenite can be grouped in to three classes: homogeneous or fresh ilmenite, ilmenite with exsolution phenomena and altered ilmenite. The ilmenite alteration takes place into

goethite, rutile, hematite and leucoxene [14], discussed the chemical composition of the highly purified ilmenite concentrate where it is composed of the following oxides: 51.55% Fe₂O₃, 43.49% TiO₂, 1.37% MnO, 0.71% MgO, 0.86% Al₂O₃, 0.24% Cr₂O₃, 0.17% V₂O₅, 0.42% CaO, 0.70% SiO₂, 0.22% P₂O₅ and traces of Nb, Co, Ni, Zn, Mo and Zr. The EDX/BSE images of Ilmenite of study area ESEM were shown in figure 13.

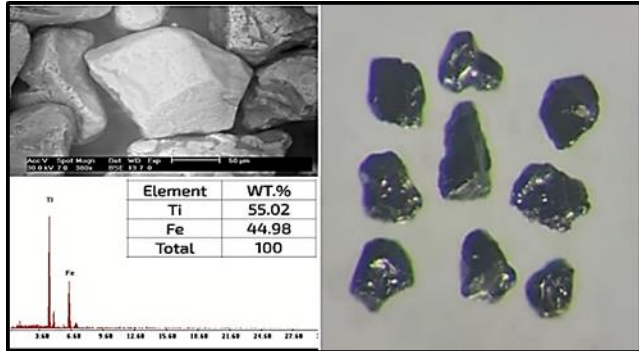


Fig. 13: EDX semi-quantitative analyses and BSE images of ilmenite Euhedral grains.

6.3 Garnet Minerals

Garnet represents 1.8 wt. % of the total economic minerals. Its content varies between 0.02 – 0.69 wt. % with average value of 0.24 wt. %. Most of the Egyptian beach garnet grains exhibit the pink, red brown, yellow orange and green colours. The pink and red colored particles are isotropic while yellow and orange ones are weakly anisotropic. Few complete euhedral rhombic dodecahedrons and trapezohedron grains were detected. [25] pointed out that the most common garnet varieties are the rosy pink and reddish pink-coloured garnets, which constitute about 80% and 18% of the bulk garnet respectively.

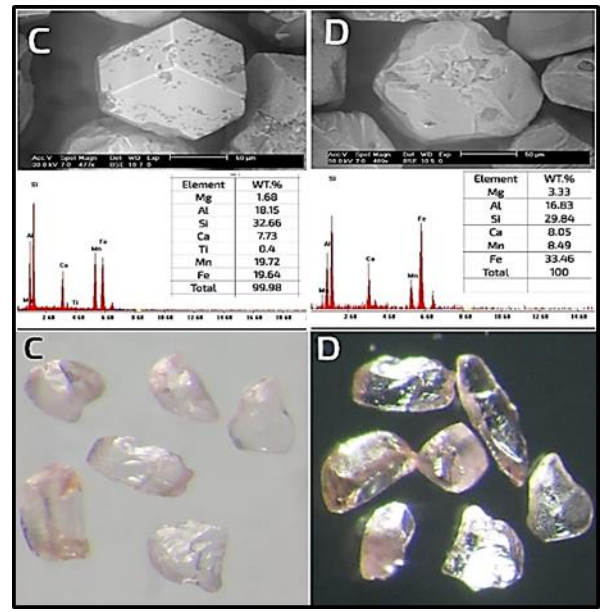
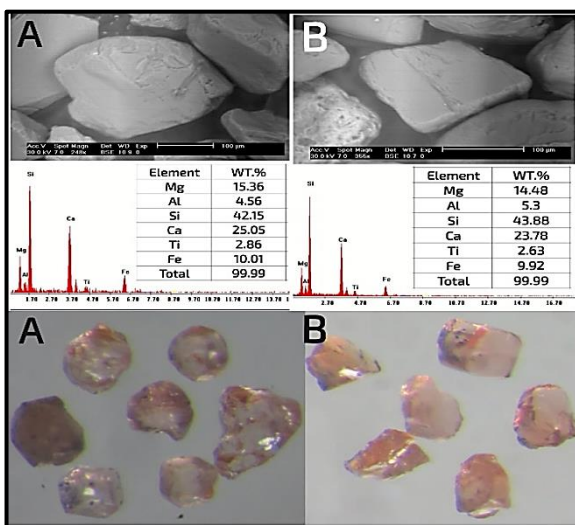


Fig. 14: (A, B, C and D) EDX semi-quantitative analyses and BSE images of Euhedral garnet crystal.

The size is relatively coarse and 80% of the garnet grains are larger than 0.250 mm in diameter. [14] showed that garnet contains 22.31% Al₂O₃, 30.67% Fe₂O₃, 0.93% MnO, 8.23% MgO, 1.98% CaO, in analyzed garnet and the trace elements are: 500 ppm Cr, 400 ppm Ga, 500 ppm Sc, 80 ppm V, 100 ppm Y, and 100 ppm Zn. The garnet is sometimes pitted and stained with iron oxide. the EDX/BSE images of garnet of study area ESEM were shown in figure 14(A and B).

6.4 Leucoxene

Leucoxene represents 8.4 wt. % of the total economic minerals. Its content varies between 0.09 – 3.97 wt. % with average value of 1.11 wt. %. Leucoxene is not a true mineral but the transition stage during the alteration of ilmenite to secondary rutile [26] and [27]. It is a mixture of pseudorutile, brookite, anatase and rutile [28] and [29]. It is recorded in the studied sediments as amorphous sub-rounded to well-rounded particles containing more than 70 % Ti O₂ with dark brown, pale brown, gray and creamy color. The variation of color is related to the iron content in the particle (Mostafa 1995). Few leucoxene particles are euhedral with the crystal form of its parent ilmenite. According to [30], the grains were investigated using the Environmental Scanning Electron Microscope (ESEM). The EDEX Semiquantitative elemental composition analysis was performed essentially for Fe, Ti, Mg, Mn, Cr, Al and Si. The majority of leucoxene present as subangular to subrounded grains, with homogenous black coloured to dark brown and light brown. the EDX/BSE images of Leucoxene of study area ESEM were shown in figure 15.

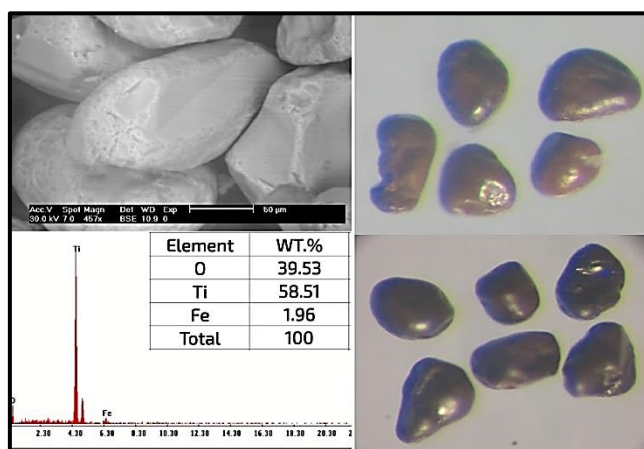


Fig.15: EDX semi-quantitative analyses and BSE images of Euhedral Leucoxene crystal.

6.5 Zircon ($ZrSiO_4$)

Zircon represents 5.7 wt. % of the total economic minerals. Its content varies between 0.06 – 3.40 wt. % with average value of 0.75 wt. %. [31], classified the Egyptian beach zircon according to shape as follows: 1) Idiomorphic (euhedral) 5.3%, 2) Subhedral 40.5% and 3) Anhedral 54.2%. Zircon is mostly recorded as bipyramidal elongated prismatic particles with almandine luster beside the needle, barrel, oval and the spherical ones. Few zircon particles with very short prism between the two pyramids were detected. Twinned zircon grains are very rare. An elbow type twined zircon has been observed. Most of the Egyptian beach zircon particles are colourless, free from inclusions while others are coloured with shades of yellow, pink, red, dark brown and smokey. The inclusions are mostly of iron oxide and are common in zircon. [32] showed that the darker zoned zircon is more radioactive than the colourless one. The zirconium content of a pure sample obtained by [33] was 48.34% Zr. According to [14] showed that zircon contains 64.47% (Zr+Hf) O₂, 31.37% SiO₂, 0.47% TiO₂, 0.35% Al₂O₃, 0.75% Fe₂O₃, 0.55% MgO, 0.37% Th O₂, 0.40% UO₂ and 0.78% RE₂O₃. The EDX/BSE images of zircon of study area ESEM were shown in figure 16(A and B).

6.6 Rutile (TiO_2)

represents 2.2 wt. % of the total economic minerals. Its content varies between 0.03 – 1.13 wt. % with average value of 0.29 wt. %. Most of the Egyptian beach rutile grains have elongated bipyramidal prisms but tabular, spherical and irregular ones are also present. Some rutile particles exhibit elbow-shaped twinning. It is generally reddish brown to foxy red in colour although black, dark brown, orange and yellow rutile grains are also observed. The Egyptian beach rutile is characterized by a considerable Nb content, which is substituting for Ti. [11]

showed that rutile contains 97.54% TiO₂, 0.31% SiO₂, 0.47% Fe₂O₃, 0.83% V₂O₅, 0.28% Nb₂O₃, 0.12% Al₂O₃, 0.10% MgO, 0.05% Cr₂O₃, and 0.30% CaO. The Egyptian beach rutile represented by two main varieties, the primary rutile formed during magmatic crystallization and secondary rutile derived from the alteration of Fe-Ti oxides especially ilmenite. The secondary rutile is the end product of the alteration of Fe-Ti oxides and is characterized by its black opaque appearance under the polarized microscope. The EDX/BSE images of rutile of study area ESEM were shown in figure 17(A and B).

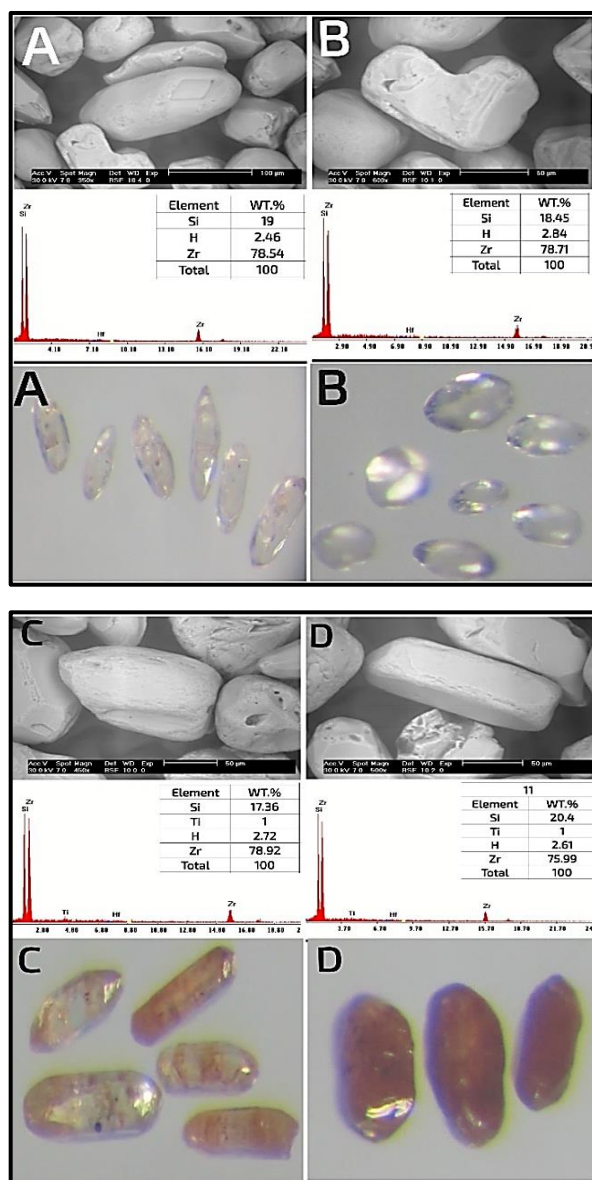


Fig. 16: A, B, C and B EDX semi-quantitative analyses and BSE images of prismatic bipyramidal zircon.

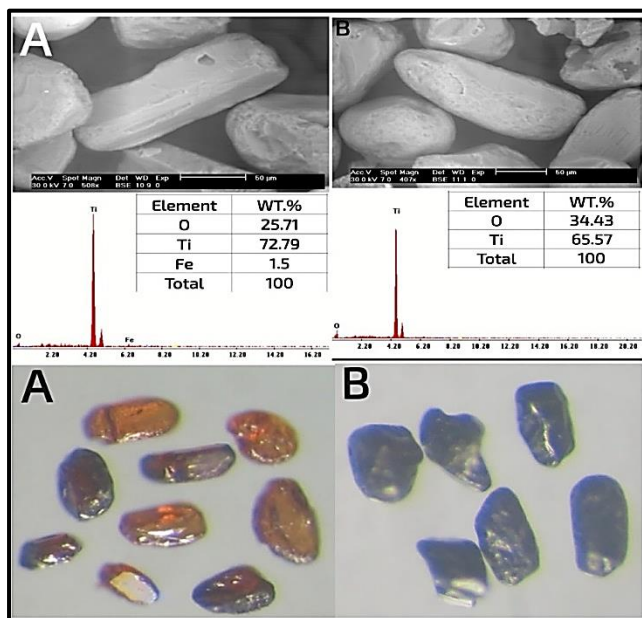


Fig.17: A and B EDX semi-quantitative analyses and BSE images of prismatic and spherical rutile grains.

6.7 Monazite (Ce, La, Nd, Pr, Th, Y) PO₄,

Monazite represents 0.35 wt. % of the total economic minerals. Its content varies between 0.003 – 0.198 wt. % with average value of 0.046 wt. %. The Egyptian beach monazite grains are generally canarian yellow, few particles exhibit yellow, lemon yellow, honey yellow, pale green and orange colours. Some grains are stained by thin films of iron oxides. The grains are pitted and have rough surfaces. Monazite grains are mostly rounded, elongated, sometimes altered and partly present in a metamict state.

The oxidation of cerium to ceric oxide during alteration and the staining and penetration of the iron oxide cause changes in coloration of some monazite grains [24] and [18]. It contains 61.5 wt. % REEs, 5.75 wt. % thorium and 0.65 wt. % uranium in addition to small contents of ferric oxide, titanium dioxide and silica. in the Egyptian beach monazite. According to [34]. The distribution of the rare earth elements is in the order of Ce > La > Nd > Pr > Sm, which is in accordance with the general trend in most reported chemical compositions of monazites. According to [35] classified the Egyptian beach monazite into six coloured varieties. The two major monazite varieties are the lemon-yellow monazite forming 59% of the total grains and the honey yellow monazite forming 25% of the total. The four minor groups are white to colourless 16%, pale green 5.5% brown 2.5% and dark orange 2%. [35] (op.cited) concluded that monazite was derived from one type of source rock namely sedimentary. Monazite can be used as a source of rare earth elements. However, monazite is present only in very small amounts in the Egyptian beach sands. Other heavy minerals (Green silicates) found at the studied area include staurolite, kyanite, sillimanite, andalusite,

calcite, biotite and tourmaline but these are which became economic importance. Both dahllite [Ca₅(PO₄, CO₃)₃(OH)] and axinite [Ca₂(Mn,Fe,Mg)Al₂(BO₃OH)(SiO₃)₄] are recorded for the first time in the present work. Pyroxenes are represented mainly by augite, diopside while hypersthene is rare. Amphiboles are represented mainly by hornblende, fibrous tremolite-actinolite and epidote. The EDX/BSE images of monazite of study area ESEM were shown in figure 18(A and B).

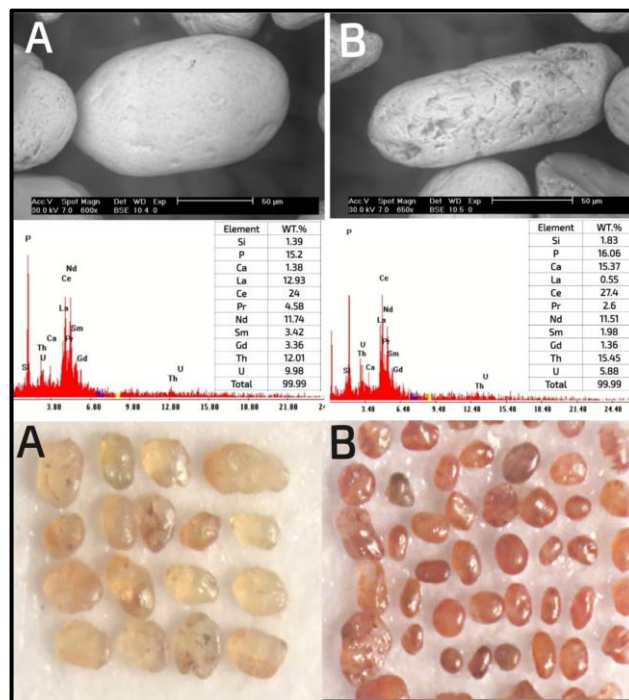


Fig. 18: (A and B) EDX semi-quantitative analyses and BSE images of subrounded monazite grains with contaminated surfaces picked.

7 Conclusions

The study area was conducted in al-Dibah beach area in Port Said governorate to detect economic minerals, 51 samples were collected from 400-meter mesh pattern parallel to the beach and 50 meters vertically on the beach to assess an area of 8 km long and a depth of 150 meters wide. Using a definite mineralogical analysis procedure program, different heavy mineral contents were calculated in the various samples collected. Using wet gravity concentration, low and high intensity magnetic separation and the high-tension electrostatic separation techniques, each of the six individual economic minerals, leucoxene and cassiterite can be obtained in a high-grade concentrate with accepted grade and recovery. The resource tonnage for each concerned economic mineral in the different sectional area is calculated for the drilled top meter depth zone to be: (92.640 ilmenite, 58.720 Magnetite, 3.840 garnet, 17.760 Leucoxene, 12.000 zircon, 4.640 rutile, 0.736 monazite and 20.960 Green silicates) a total reserve of thousand tons. Average concentrations (eU unit, ppm (eTh) is up to 1.41

and 4.66 ppm, respectively. In addition, the concentration of potassium (K, %), averages 0.60%. The absorbed dose calculation values were also found to range from 6.47 to 32.22 (nGy/h) with an average value of 21.54 (nGy/h). This is lower than the global average value of 60 nGy/h (UNSCEAR 2000), and the average total effective dose value of all terrestrial gamma rays is 0.174 (mSv/y).

Acknowledgement

The authors would like to express their respectful thanks and sincere gratitude to Professor Dr Mohamed. G. El Feky Professor of Geo-chemistry for his continuous support

References

- [1] El-Askary, M.A. and Frihy, O.E: Depositional phases of Rosetta and Damietta promontories on the Nile Delta Coast. *Jour. African earth Sci., Great Britain.,* **5(6)**, 627- 633,1986
- [2] El-Hadary AF: Geological, sedimentological and radiometric studies on the black sand deposits, west Rosetta beach with emphasis on the heavy economic minerals. Ph.D. Thesis, Fac. Sci., Cairo Univ., Egypt., 1998.
- [3] Higazy AK, Emam MH: Accumulation and soil to plant transfer of radionuclides in the Nile Delta coastal black sand habitats. *International Journal of phytoremediation.,* **13**: 140-155, 2011.
- [4] Gindy AM: Radioactivity in monazite, zircon and radioactive black grains in black sands of Rosetta, Egypt. *Econ. Geol.,* **56**, 257–259,1961.
- [5] Meshref WM: Mineralogical and radiometric study for some black sand deposits on the Mediterranean coast. M.Sc. Thesis, Fac. Sci., Ain Shams University, Cairo, Egypt., 1962.
- [6] Hammoud NMS, Khazback AE: Relative radiometric assay of Egyptian beach monazite. *Mineralia Slovaca.,* **5**, 469–475, 1973.
- [7] Meleik ML, Fouad KM, Wassef SN, Ammar AA, Dabbour GA: Aerial and ground radiometry in relation to the sedimentation of radioactive minerals of the Damietta beach sand, Egypt. *Econ. Geol.,* **73**, 1738–1748, 1978.
- [8] El-Shazly EM, El Sokkary AA, Dabbour GA: Physical properties of beach zircon from the Mediterranean Sea coast of Egypt, Part I Grain size, Shape and roundness. *Egypt, J. Geol.,* **25**, 95–111, 1981.
- [9] Dabbour GA, Morsy MA, Kamel AF: Radioactivity and heavy economic minerals of some Quaternary sediments at El Arish beach, north Sinai, Egypt. *Ann., Geol. Surv. Egypt.,* **16**, 51 – 56, 1988.
- [10] Moustafa, M. I.: Investigations of some physical properties of zircon and rutile to prepare high purity mineral concentrates from black sand deposits, Rosetta, Egypt. M.Sc. Thesis, Fac. Sci., Mansoura Univ., Egypt., **140**, 1995.
- [11] Moustafa MI: Mineralogy and beneficiation of economic minerals in the Egyptian black sands. Ph.D. Thesis, Fac. Sci., El Mansoura University, El Mansoura, Egypt., **316**, 1999.
- [12] Moustafa, M.I.; Hegab, O.A. and El Agami, N.L.: Remarks on the physical, mineralogical features and amenability of separation of rare accessory minerals from the black sands of the northern coast of Egypt, *Egyptian Mineralogist.,* **12**, 29-49, 2000.
- [13] Barakat, M.G.: Sedimentological studies and evaluation of some black sand's deposits on the northern coast of Egypt. M.Sc. Thesis, Fac. Sci. Alex. Univ., Egypt, 176 p, 2004.
- [14] Barakat, M.G: Evaluation and mineralogy of beach economic minerals especially ilmenite for the top meter in the Egyptian black sand, east Rosetta, Egypt. Ph. D. thesis: Fac. Sci. Zagazig University., 317, 2016.
- [15] El-Kammar, A.A., Ragab A.A. and Moustafa, M.I.: Geochemistry of economic heavy minerals from Rosetta black sand of Egypt. *Journal of KAAL: Earth Sciences, Kingdom of Saudi Arabia.,* **22(2)**, 1-25, 2010.
- [16] El-Gamal, A. and Saleh, I.H. (2012): Radio logical and mineralogical investigation of accretion and erosion coastal sediments in Nile Delta region, Egypt. *Journal of oceanography and Mar. Sci.,* **3(3)**, 41-55.
- [17] El-Shafey A. M: Mineralogical, evaluation and beneficiation of the economic minerals of Egyptian black sands especially Cassiterite, in Abu-Khashaba area, east Rosetta, Egypt. M.Sc. Thesis, Fac. Sci. Zagazig University., 132, 2011.
- [18] El-Shafey A. M: Upgrading and mineralogical studies for some Economic and nuclear Elements Bearing Minerals of Rosetta black deposits, Egypt, with especial emphasis on Monazite. Ph. D. thesis: Fac. Sci. Zagazig University., 172, 2016.
- [19] Wassef SN: Correlation of the sedimentation conditions of the Mediterranean beach east of Damietta to Suez Canal by heavy minerals and isotope applications. M.Sc. Thesis, Fac. Sci., Ain Shams Univ., Egypt, 1964.
- [20] HAM Awad, HMH Zakaly, AV Nastavkin, A. El-Taher Radioactive content and radiological implication in granitic rocks by geochemical data and radiophysical factors, Central Eastern Desert, Egypt *International Journal of Environmental Analytical Chemistry.,* 1-14, 2020.
- [21] El-Taher, A, L Najam, I Hussian, MA Ali Omar Evaluation of natural radionuclide content in Nile River sediments and excess lifetime cancer risk associated with gamma radiation. *Iranian Journal of Medical Physics.,* **16(1)**, 27-33, 2019.
- [22] Hashem A Madkour, Mohamed Anwar K Abdelhalim, Kwasi A Obirikorang, Ahmed W Mohamed, Abu El-Hagag N Ahmed, A El-Taher, Environmental implications of surface sediments from coastal lagoons in the Red Sea coast *Journal of Environmental Biology.,* **36(6)**, 1421, 2015.
- [23] UNSCEAR: Sources and effects of ionizing radiation. Report to the General Assembly of the United Nations with Scientific Annexes, United Nations sales publication E.00.IX.3, New York, 2000.
- [24] Hammoud, N.M.S.: Concentration of monazite from Egyptian black sands employing industrial techniques. M.Sc. Thesis, Fac. Sci., Cairo Univ., Cairo, Egypt., 198, 1966.
- [25] Dewedar, A.A.: Comparative studies on the heavy minerals in some black sands deposits from Sinai and east Rosetta with contribution to the mineralogy and economics of their garnets. Ph.D. Thesis, Fac. Sci., El Menoufia Univ., Shebin El Koum, Egypt., 197, 1998.
- [26] Milner, H.B.: Sedimentary petrology. George Allen and Unwin LTD., 137, 1962.
- [27] Ramdohr, P.: The ore minerals and their intergrowths. English Translation of the 4th ed. Pergamon Press, Oxford., 1174, 1980.
- [28] Frost, M.T.; Grey, I.E.; Harrowfield, I.R. and Mason, K.: The dependence of alumina and silica contents on the extent of alteration of weathered ilmenites from Western Australia. *Mineral. Mag.,* **47**, 201-208, 1983.
- [29] Force, E.R.: Geology of titanium mineral deposits. *Geol. Soc. Am.,* **259**, 78, 1991.

- [30] Abdel-Fattah, M. F.: Evaluation, beneficiation and mineralogy of the Egyptian beach leucoxene in Abu Khashaba area, east Rosetta, Egypt. M.Sc. Thesis, Fac.Sci. Zagazig University, Egypt., 152, 2008.
- [31] Madkour, M Tamam, Atef El-Taher, Gharam A Alharshan, Mostafa YA Mostafa an extended assessment of natural radioactivity in the sediments of the mid-region of the Egyptian Red Sea Coast Marine Pollution Bulletin., **171**, 112658, 2021.
- [32] Gindy, A. M.: Radioactivity in monazite, zircon and radioactive black grains in black sands of Rosetta, Egypt. Econ. Geol., **56**, 257–259, 1961.
- [33] Abdel Gawad, A.M.: X-ray spectrographic determination of hafnium-zirconium ratio in zirconium minerals, Am. Min., **51**, 464-473, 1966.
- [34] Moustafa, M.I.: Mineralogical characteristics of the separated magnetic rutile of the Egyptian black sands. Resource geology, Vol. 60, Is., **3**, 300-312, 2010.
- [35] Zaghoul, Z.M. and Kamel, K.: The mineralogical and Petro – graphical features of monazite from the black sands of Rosetta. J. Geol. U.A.R., **9(1)**, 17–31, 1965.